Modulating mutational outcomes and improving precise gene editing at CRISPR-Cas9-induced breaks by chemical inhibition of end-joining pathways

Schimmel, J.; Munoz Subirana, N.; Kool, H.; Schendel, R. van; Vlies, S. van der; Kamp, J.A.; ... ; Tijsterman, M.

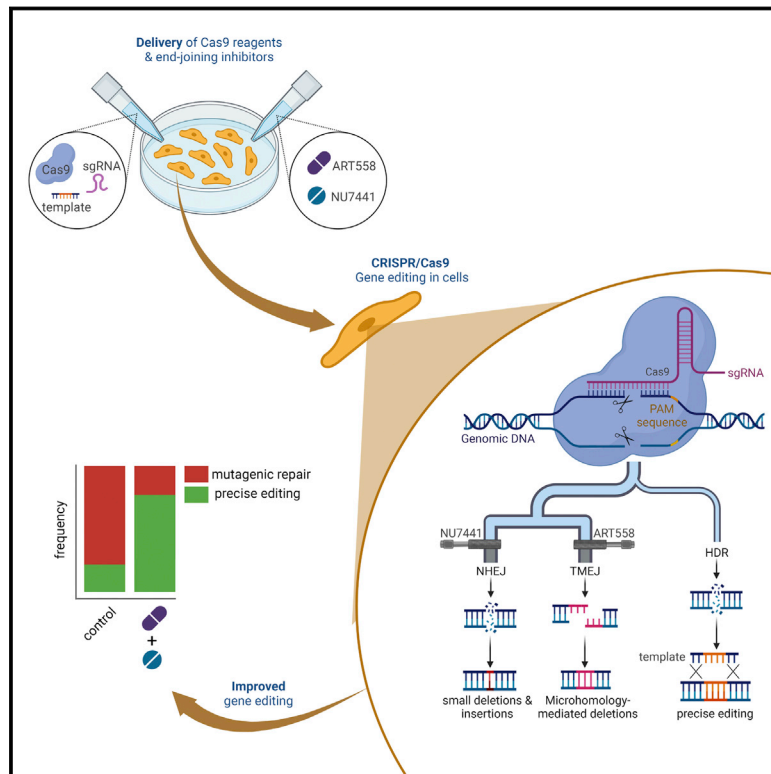# Modulating mutational outcomes and improving precise gene editing at CRISPR-Cas9-induced breaks by chemical inhibition of end-joining pathways

Graphical abstract

Authors

Joost Schimmel, Núria Muñoz-Subirana, Hanneke Kool, ..., Graeme C.M. Smith, Simon J. Boulton, Marcel Tijsterman

Correspondence

m.tijsterman@lumc.nl

In brief

Precise gene editing is severely impeded by highly efficient and mutagenic end-joining repair of CRISPR-Cas9-induced breaks. Here, Schimmel et al. provide a robust and easy strategy to improve the fidelity and safety of genome engineering by combined chemical inhibition of the two main end-joining pathways.

Highlights

- ART558 is a potent inhibitor of TMEJ at CRISPR-Cas9-induced chromosomal breaks

- Inhibition of TMEJ by ART558 prevents large deletions at CRISPR-Cas9-induced breaks

- Dual inhibition of TMEJ and NHEJ improves the efficiency of precise gene editing

Report

Modulating mutational outcomes and improving precise gene editing at CRISPR-Cas9-induced breaks by chemical inhibition of end-joining pathways

Joost Schimmel,[1,7] Núria Muñoz-Subirana,[1,7] Hanneke Kool,[1] Robin van Schendel,[1] Sven van der Vlies,[1] Juliette A. Kamp,[2] Femke M.S. de Vrij,[2] Steven A. Kushner,[2,3] Graeme C.M. Smith,[4] Simon J. Boulton,[4,5] and Marcel Tijsterman[1,6,8,*]

[1]Department of Human Genetics, Leiden University Medical Center, Leiden, the Netherlands
[2]Department of Psychiatry, Erasmus Medical Center, Rotterdam, the Netherlands
[3]Department of Psychiatry, Columbia University Irving Medical Center, New York, NY, USA
[4]Artios Pharma, The Glenn Berge Building, Babraham Research Campus, Cambridge, UK
[5]The Francis Crick Institute, London, UK
[6]Institute of Biology Leiden, Leiden University, Sylviusweg 72, 2333 BE Leiden, the Netherlands
[7]These authors contributed equally
[8]Lead contact
*Correspondence: m.tijsterman@lumc.nl
https://doi.org/10.1016/j.celrep.2023.112019

SUMMARY

Gene editing through repair of CRISPR-Cas9-induced chromosomal breaks offers a means to correct a wide range of genetic defects. Directing repair to produce desirable outcomes by modulating DNA repair pathways holds considerable promise to increase the efficiency of genome engineering. Here, we show that inhibition of non-homologous end joining (NHEJ) or polymerase theta-mediated end joining (TMEJ) can be exploited to alter the mutational outcomes of CRISPR-Cas9. We show robust inhibition of TMEJ activity at CRISPR-Cas9-induced double-strand breaks (DSBs) using ART558, a potent polymerase theta (PolΘ) inhibitor. Using targeted sequencing, we show that ART558 suppresses the formation of microhomology-driven deletions in favor of NHEJ-specific outcomes. Conversely, NHEJ deficiency triggers the formation of large kb-sized deletions, which we show are the products of mutagenic TMEJ. Finally, we show that combined chemical inhibition of TMEJ and NHEJ increases the efficiency of homology-driven repair (HDR)-mediated precise gene editing. Our work reports a robust strategy to improve the fidelity and safety of genome engineering.
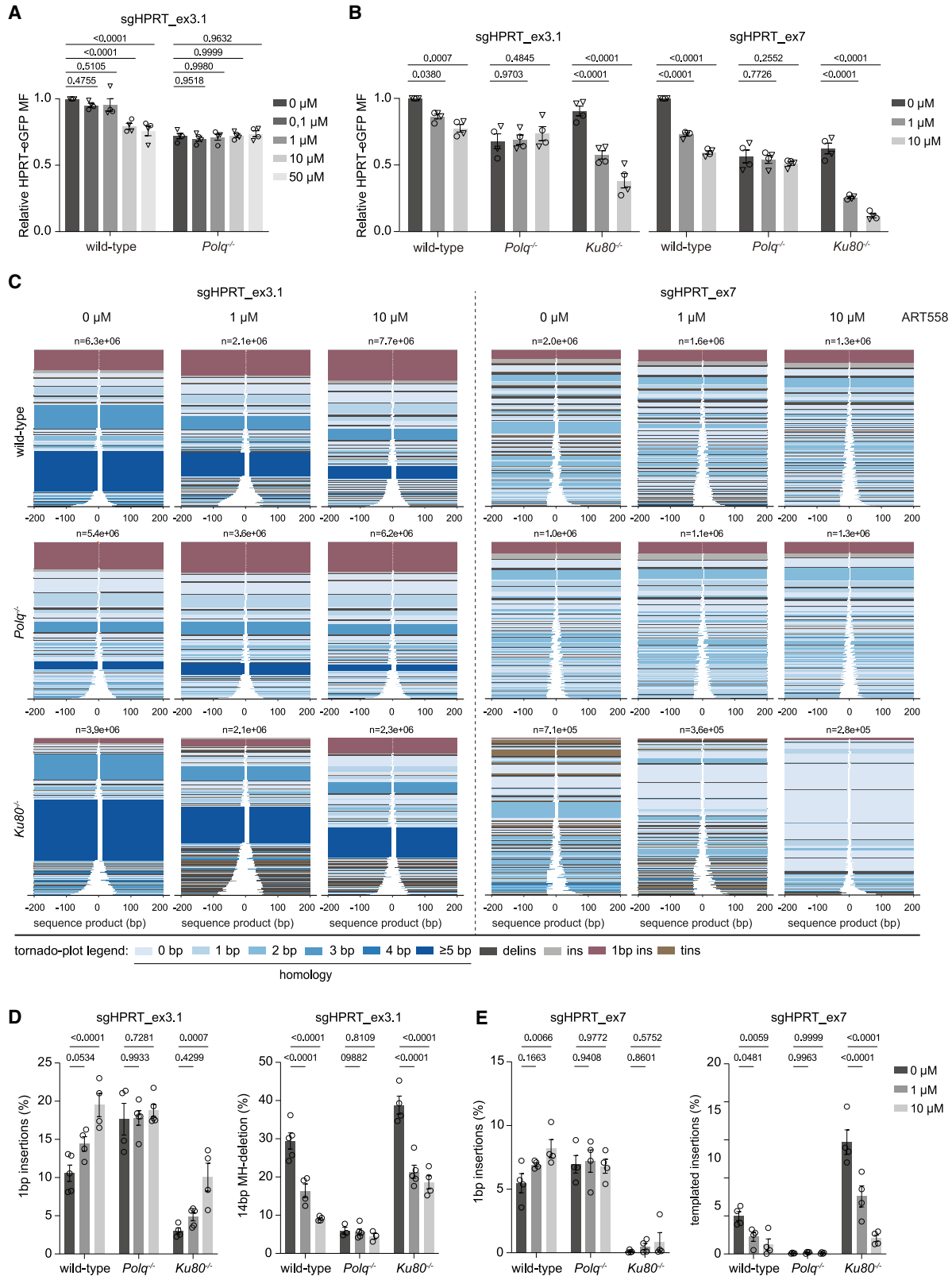
INTRODUCTION

Manipulation of genomes by CRISPR technology is brought about either by uncontrolled or by sequence-guided repair of Cas9-induced double-strand breaks (DSBs).[2] Precise gene editing can be achieved by co-delivery of exogenous donor DNA that can serve as a template for homology-driven repair (HDR) at these DSBs. However, the prevalence of deletions and/or insertions generated by mutagenic end joining of Cas9-induced DSBs hampers high-fidelity modification of the genome.[3–5] Moreover, mutagenic repair leading to large deletions, chromosomal translocations, and even integration of delivery reagents at on- and off-target sites poses a significant safety risk for future clinical applications.[6,7] Large deletions and gross chromosomal rearrangements also complicate the interpretation of gene-editing experiments [8–13] as these alterations are often difficult to recognize in diagnostic schemes. Because of these risks, additional CRISPR-Cas9 strategies are being developed based on nuclease-impaired Cas9 enzymes to bypass the need to introduce DSBs for gene ed-

iting.[14–17] Despite their potential, the previous and improved strategies based on Cas9-induced DSBs often outcompete these strategies, mostly due to efficiency, and hence remain the most widely used technique to generate knockin and knockout genetic models.[18–20]

Over the last few years, efforts have focused on increasing the frequency of HDR usage at Cas9-induced breaks, ranging from rational design of the repair template and development of HDR-stimulating Cas9-protein fusions to the specific induction of breaks during S-G2 phases of the cell cycle when HDR is most active.[21–25] More indirectly, inhibition of mutagenic end joining has also been suggested as a strategy to improve the efficiency of precise gene editing. However, attempts to suppress mutagenic repair of Cas9-induced breaks by inhibiting the core NHEJ factors DNA-PKcs and LigIV has thus far revealed variable effects on gene editing, partly depending on cell type and culturing conditions (reviewed in Yeh et al.[25]). The lack of a consistent effect on HDR upon NHEJ inhibition may be due to the existence of a second end-joining pathway, termed theta-mediated end joining (TMEJ),

A sgHPRT_ex3.1

B sgHPRT_ex3.1   sgHPRT_ex7

C sgHPRT_ex3.1   sgHPRT_ex7   ART558

0 µM   1 µM   10 µM   0 µM   1 µM   10 µM

tornado-plot legend: 0 bp 1 bp 2 bp 3 bp 4 bp ≥5 bp   delins   ins   1bp ins   tins
                              homology

D sgHPRT_ex3.1   sgHPRT_ex3.1   **E** sgHPRT_ex7   sgHPRT_ex7

(legend on next page)

which is a prominent contributor to mutagenic repair of DSBs and CRISPR-Cas9-induced chromosomal lesions in different species.[26–30] In contrast to NHEJ, this intrinsically mutagenic repair pathway is sequence guided, relying on the annealing of small stretches of identical sequences present at either side of the DSB (i.e., microhomology) to guide repair.[31] Since small-molecule inhibitors of TMEJ were unavailable until recently, genetic knockout or transient knockdown of its key factor, polymerase theta (Polθ; encoded by the *Polq* gene), was used to show that loss of this pathway enhances CRISPR-Cas9-mediated HDR.[32,33]

Here, we examine how chemical inhibition of NHEJ and TMEJ with small molecules affects the outcome of mutagenic repair at CRISPR-Cas9-induced DSBs. To this end, we validate the recently developed Polθ inhibitor ART558[34] on mouse and human cells and analyzed CRISPR-Cas9-induced mutational signatures at different target sites. ART558 has been shown to block Polθ's polymerase activity by stabilizing its closed conformation while bound to DNA.[35] We find that treatment of cells with ART558 phenocopies a genetic *Polq* knockout; inhibition of TMEJ strongly suppresses microhomology-dependent deletion formation. Conversely, NHEJ inhibition shifts the mutation spectrum in an opposite direction toward microhomology-mediated repair products and triggers the formation of an unappreciated class of large kb-sized deletions, which are suppressed by ART558. Finally, we show that inhibition of TMEJ with ART558 increases the efficiency of HDR-mediated repair on Cas9-induced DSBs, most profoundly in combination with a NHEJ/DNA-PKcs inhibitor. Together, our data demonstrate the utility of small-molecule EJ inhibitors to modulate the mutational outcome of CRISPR-Cas9 approaches to reduce excessive deletions and to promote HDR. In addition, our work warrants further investigation into the use of Polθ inhibitors in future clinical gene-editing approaches, broadening its use beyond that of anti-cancer therapy.

RESULTS

ART558 reduces mutagenic repair at Cas9-induced breaks in mouse embryonic stem cells

Recently, a potent and specific Polθ inhibitor, termed ART558, was reported that elicits synthetic lethality in homologous-recombination-deficient cells without perturbing growth in isogenic wild-type cells.[34] To investigate the efficacy and specificity of ART558 in targeting TMEJ of Cas9-induced breaks, we pre-treated wild-type and Polθ-deficient (*Polq*$^{-/-}$) mouse embryonic stem cells (mESC) with different concentrations of ART558, after which we introduced a blunt DSB in the selectable marker gene *HPRT-EGFP* (Figure S1A).[36] We found that ART558 showed maximal reduction of Cas9-induced mutation frequency at 10 μM in wild-type cells without having an additional effect on the already reduced mutation frequency observed in Polθ-deficient cells (Figure 1A). Next, we validated this finding by targeting four different sites in *HPRT-EGFP* (designated HPRT_ex2, HPRT_ex3.1, HPRT_ex3.2, and HPRT_ex7, Figure S1A) in cells treated either with 0, 1, or 10 μM ART558. We also tested NHEJ-deficient *Ku80*$^{-/-}$ knockout cells in which mutagenic repair of DSBs is primarily mediated by TMEJ.[26,27] For all four target sites, we observed a dose-dependent decrease of the mutation frequency in wild-type and NHEJ-deficient cells; again, ART558 exposure had no effect on the Cas9-induced mutation frequency in *Polq* knockout cells (HPRT_ex3.1 and HPRT_ex7, Figure 1B; HPRT_ex2 and HPRT_ex3.2, Figure S1B).

To carefully inspect the suggested reduction of TMEJ activity by the Polθ inhibitor, we performed targeted sequencing on ∼200 bp amplicons obtained from cells of different genetic backgrounds treated with or without ART558 and transfected with either single guide RNA (sgRNA) HPRT_ex3.1 or sgRNA HPRT_ex7. The next-generation sequencing (NGS) data was subsequently bio-informatically processed using recently developed Sequence Interrogation and Quantification (SIQ) software to produce insightful tornado plots (Figure 1C).[1] Such plots visualize all repair outcomes derived from a given cell population (10^5–10^6 cells/population), with deletions represented by a white space and the remaining DNA flanking the deletion color coded with respect to microhomology at the deletion junctions (in shades of blue). The flanks of deletions that also contain insertions are differently color coded as brown, when the insert could be mapped to a sequence also present in the flank of the deletion, and gray, when this could not be done, frequently because the insert was too small and could not be distinguished from similarity to the flanking sequence. Figure 1C shows tornado plots of the two target sites that, out of the 4 tested, contain the most (ex3.1) and least (ex7) availability of ∼3–6 bp microhomologies at either flank near the DSB end. Such small direct repeats can serve as a primer for Polθ action, guiding TMEJ repair and deletion of the intervening sequence; cNHEJ is *grosso modo*

Figure 1. ART558 treatment reduces mutagenic repair at Cas9-induced DSBs

(A) Relative HPRT-EGFP mutation frequency (MF) of wild-type and *Polq*$^{-/-}$ mESC lines transfected with Cas9-wild type (WT) and sgHPRT_ex3.1 and treated with different doses of ART558. The data shown represent the mean ± SEM (n = 4, two independent clones were used per genotype represented by different symbols) and are expressed as a fraction of the MF observed in WT cells (set to 1).

(B) Relative HPRT-EGFP MF for the indicated mESC lines transfected with Cas9-WT and sgHPRT_ex3.1 or sgHPRT_ex7 and treated with 0, 1, or 10 μM ART558. The data shown represent the mean ± SEM (n = 4) and are expressed as a fraction of the MF observed in WT cells (set to 1).

(A and B) Statistical significance was calculated via unpaired t test.

(C) Mutational signatures at Cas9-induced DSBs for the indicated mESC lines transfected with Cas9-WT and sgHPRT_ex3.1 or sgHPRT_ex7 and treated with 0, 1, or 10 μM ART558. Cells were collected for DNA extraction and used for short-read (∼200 bp) targeted sequencing around the break site. Data are represented as tornado plots where the height of each bar reflects the contribution of each outcome to the total amount of reads (n). Data are plotted relative to the Cas9-WT break site (0) and sorted by deletion size. Templated insertions (tins; see STAR Methods), 1 bp insertions, insertions, and deletion insertions (delins) are color coded. The degree of blue coloring reflects the extent of microhomology used for deletion formation. Data are the average of independent experiments (n = 4).

(D) Quantification of specific mutational outcomes from target site sgHPRT_ex3.1 for 1 bp insertions (left panel) and a microhomology-driven 14 bp deletion (right panel).

(E) Quantification of specific mutational outcomes from target site sgHPRT_ex7 for 1 bp insertions (left panel) and tins (right panel). Data are the average ± SEM (n = 4–5, as indicated). Statistical significance was calculated via two-way ANOVA multiple comparisons with Dunnett's test, comparing means of treated cells with the mean of untreated (DMSO) cells. p values are indicated in the figure panels.

A

B

C
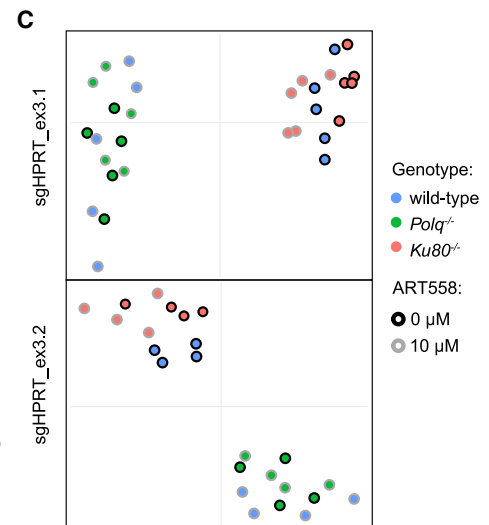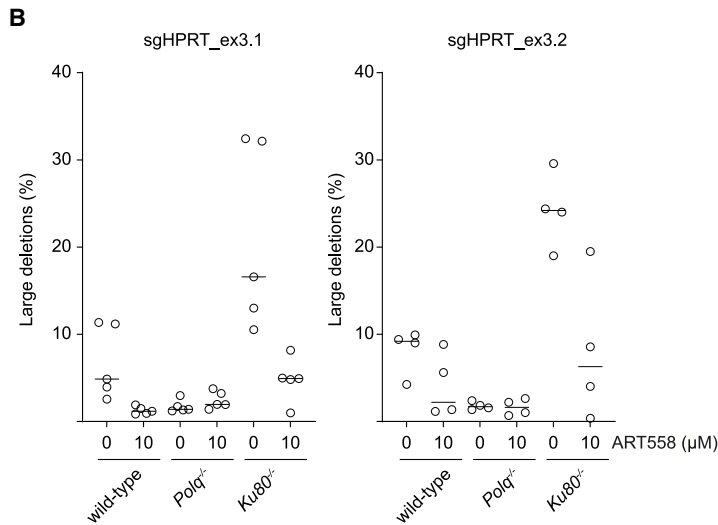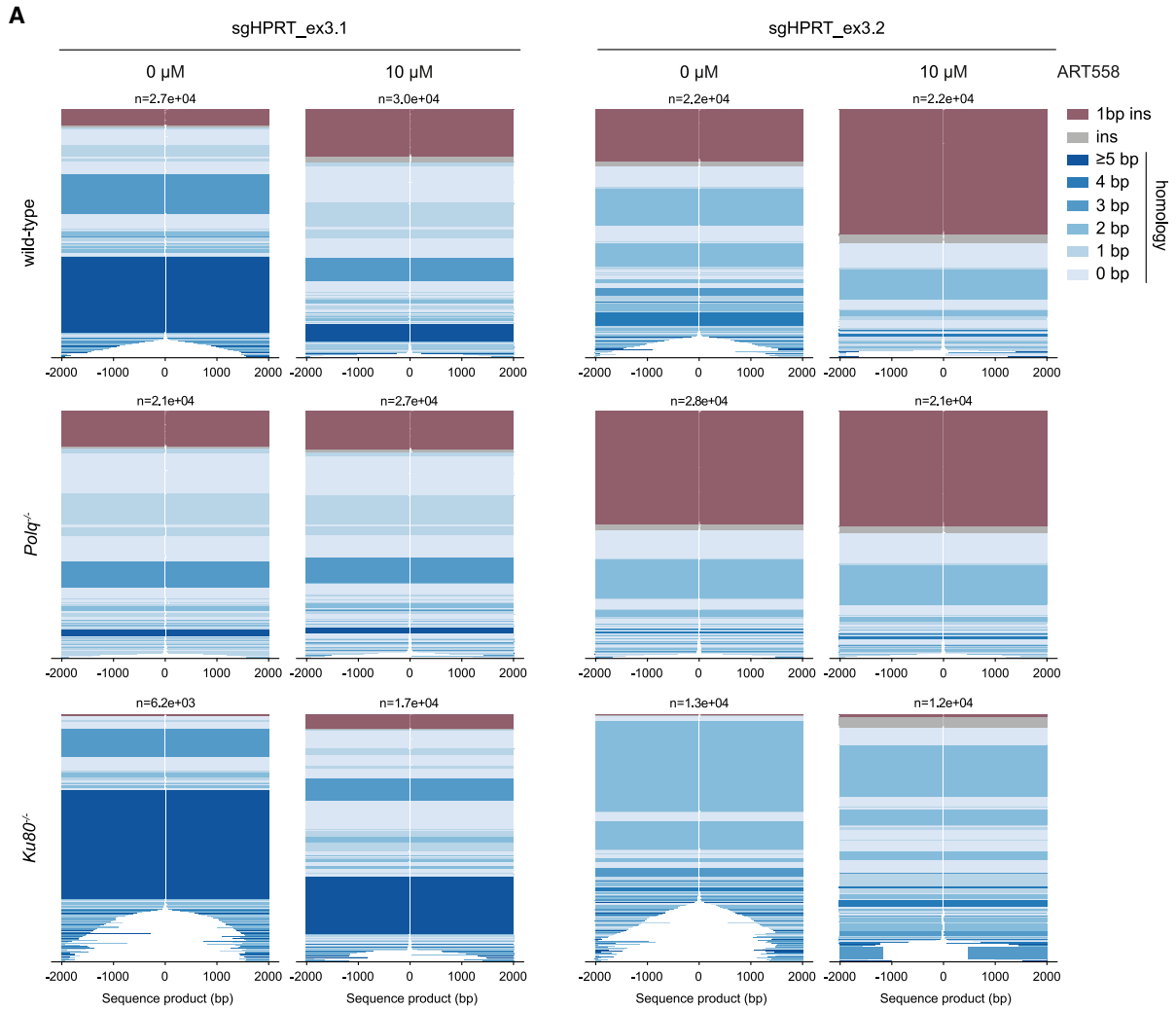
(legend on next page)

independent of sequence context. Prominence of TMEJ repair thus manifests clearer at break sites that allow for annealing of complementary DNA stretches, such as target ex3.1. For DSB sites devoid of small direct repeats in close vicinity to the break ends (such as ex7), both EJ pathways produce remarkably similar deletion mutations. However, only TMEJ produces deletions containing templated insertions, yet these represent only a minor fraction of the total TMEJ activity (Figure S1C) and appear to be sequence context dependent.[31] While the mutation profiles at different sites can thus be quite dissimilar, the mutation frequency measurements indicate that the overall contribution of TMEJ and NHEJ to each of them is comparable.

By comparing tornado plots, as well as extracted feature-based quantifications, such as the degree of microhomology present at the deletion junction and the percentage of events containing mappable templated insertions (Figures S1C and S1D), we conclude that ART558 strongly and specifically inhibits TMEJ at CRISPR-Cas9-induced DSBs: we find that the mutation profile of wild-type cells treated with 10 μM ART558 resembles that of $Polq^{-/-}$ cells. For HPRT_ex3.1, this profile has greatly reduced levels of otherwise prevalent microhomology flanking deletions (Figure 1D, right panel). Instead, it is enriched for 1 bp insertions (Figure 1D, left panel), which is a preferential outcome of NHEJ. For HPRT_ex7, which is not suitable to address microhomology usage (due to lack of DSB-flanking microhomologous sequences) but a better target to address templated insertion repair, we also find TMEJ to be strongly suppressed by ART558 in wild-type cells (Figure 1E, right panel) at the expense of an increase in 1 bp insertions (Figure 1E, left panel). Analyzing the top 5 mutagenic outcomes of each target site shows clear genotype-specific responses to ART558 treatment (Figures S1E and S1F). Furthermore, in $Ku80^{-/-}$ cells, in which TMEJ makes up for the majority of mutagenic repair[26,27] (Figures 1B and S1B), we found a reduction of typical TMEJ outcomes upon exposure to ART558. The residual mutagenic repair observed in this context may be explained in part by not being able to eliminate all TMEJ activity. However, the profile at target site HPRT_ex7 also points to an EJ-repair capacity independent of Polθ as well as KU80: the tornado plot of ART558-treated $Ku80^{-/-}$ cells (for visualization purposes set to 1 despite cells having a strongly reduced mutation frequency; Figure 1C) reveals that the majority of insertions or deletions (indels) are small and lack microhomology usage, which is atypical for TMEJ (Figure S1F).

Polθ inhibition prevents large deletions at CRISPR-Cas9-induced breaks

Further inspection of TMEJ products (in $Ku80^{-/-}$ cells) and NHEJ outcomes (in $Polq^{-/-}$ cells or ART558-treated cells) suggest that

TMEJ results in greater loss of DNA flanking Cas9-induced DSBs than NHEJ. This difference cannot solely be explained by a need for microhomologous sequences in the flanks, especially not for deletions that are 50–150 bp in size: microhomologous sequence stretches (e.g., of 3 bp) are abundantly present if the search space is set to 50 bp either side of the break site. We realized that the mild increase in DNA loss in TMEJ outcomes may be underestimated as we have used a relatively small amplicon (∼200 bp; Figure 1) in our NGS approach. Therefore, to test the effect of Polθ involvement in, and the ability of ART558 to suppress, the generation of larger deletions that have previously been described for CRISPR-Cas9,[10–13,37] we used PacBio sequencing of larger amplicons. We amplified a 3.5 kb region that includes HPRT exon 3 from pools of HPRT mutant cells targeted with HPRT_ex3.1 or HPRT_ex3.2 sgRNA (Figure S2A) and used SIQ to process and characterize PacBio-generated NGS data.[1]

For target site HPRT_ex3.1, we found up to ∼11% of the PacBio sequence reads in untreated wild-type cells to contain events that extend across the previously used NGS primer binding sites, representing deletions ranging from 65 to ∼2,900 bp (for simplicity termed "large deletions"). Strikingly, in Ku80-deficient cells, the fraction of these outcomes increased to ∼30%–35%. In agreement with these events being the products of TMEJ, we find that ART558 treatment prevents the formation of these large deletions in both wild-type and $Ku80^{-/-}$ cells without further affecting the mutagenic outcome of Polθ-deficient cells, where large deletions on average represent ∼2% of the total spectrum (Figures 2A and 2B). Analysis of target site HPRT_ex3.2 revealed very similar outcomes (Figures 2A, 2B, S2B, and S2C). Besides the profound inhibitory effect of ART558 on the formation of large deletions, inhibition of Polθ is also evident from the strong increase in NHEJ-dependent 1 bp insertions on this target site. To better compare how ART558 affects the mutation profile at DSBs, we performed dimensional reduction via uniform manifold approximation and projection (UMAP) on the repair outcomes of target sites HPRT_ex3.1 and HPRT_ex3.2. This analysis confirmed that wild-type cells treated with ART558 for CRISPR-induced mutagenesis behave as Polθ-deficient cells (Figure 2C).[38]

Small-molecule inhibition of TMEJ and NHEJ in human cells

Having demonstrated that ART558 treatment robustly and specifically inhibits TMEJ at CRISPR-Cas9-induced breaks in diploid, karyotype-stable yet fast-cycling mESCs, we next wished to assay human cells. We first determined the mutation profile for 5 target sites in the human HPRT gene in HEK293T

Figure 2. Large deletions at CRISPR-Cas9-induced breaks can be prevented by Polθ inhibition

(A) Mutational signatures at Cas9-induced DSBs for the indicated mESC lines treated with 0 or 10 μM ART558 and transfected with Cas9-WT and sgHPRT_ex3.1 or sgHPRT_ex3.2. 6-TG resistant (HPRT mutant) cells were collected for DNA extraction and used for long-read (∼3,500 bp) targeted sequencing around the break site. Data are represented as tornado plots where the height of each bar reflects the contribution of each outcome to the total amount of reads (n). Data are plotted relative to the Cas9-WT break site (0) and sorted by deletion size. Insertions, 1 bp insertions, and the extent of microhomology used for deletion formation are color coded. Data are the average (sgHPRT_ex3.1, n = 5, sgHPRT_ex3.2, n = 4).

(B) Quantification of the percentage of large deletions (see main text for definition) observed in long-read sequencing of indicated samples. Individual data points are represented, and the median is indicated.

(C) UMAP embedding of the top 50 of all mutational outcomes from (A) colored by genotype and treatment (0 or 10 μM ART558) for sgHPRT_ex3.1 and sgHPRT_ex3.2.
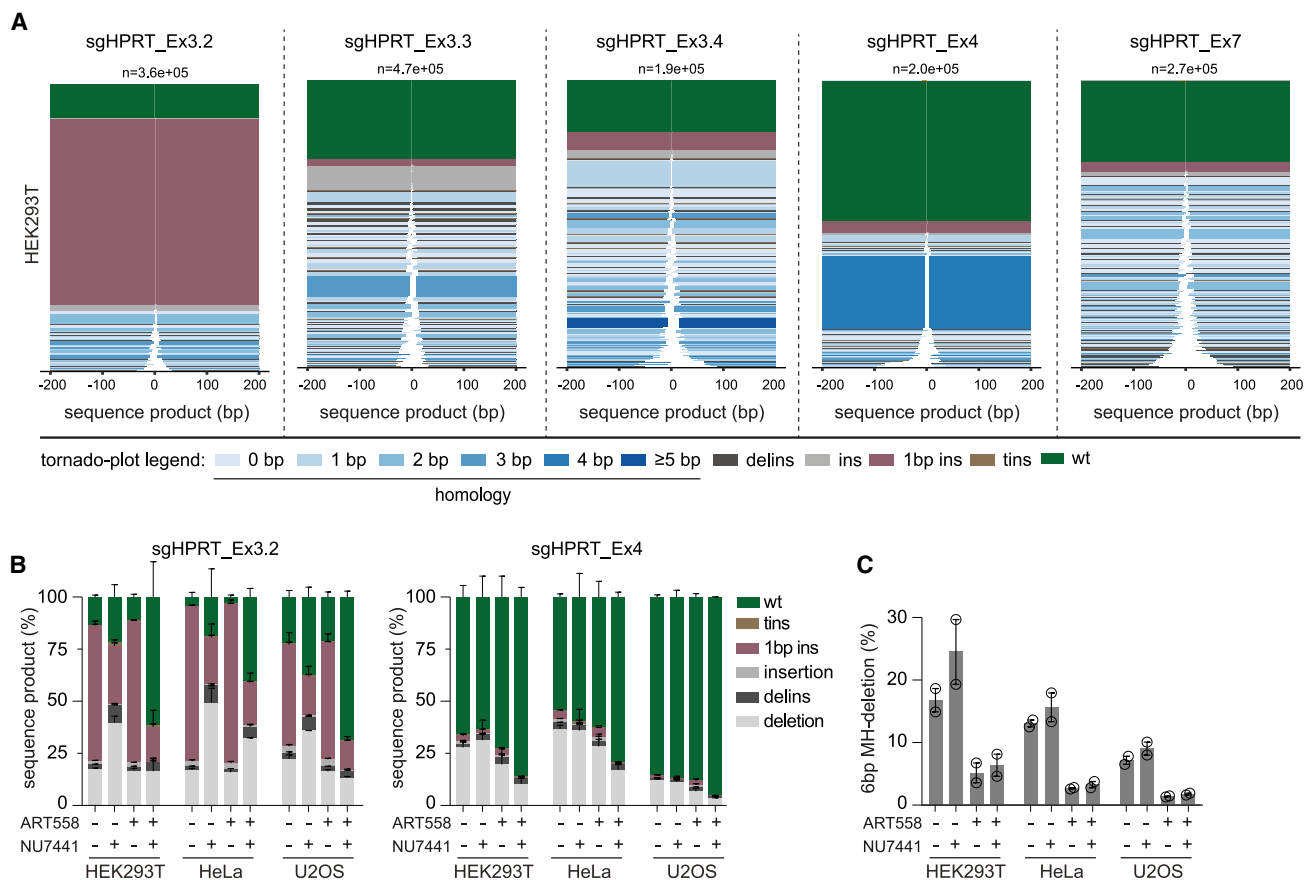
**Figure 3. Mutational signatures at Cas9-induced breaks in human cells treated with ART558 and NU7441**

(A) Mutational signatures at Cas9-induced DSBs from HEK293T cells transfected with Cas9-WT and indicated HPRT sgRNAs. Cells were collected for DNA extraction and used for short-read (∼200 bp) targeted sequencing around the break site. Data are represented as tornado plots where the height of each bar reflects the contribution of each outcome to the total amount of reads (n). Data are plotted relative to the Cas9-WT break site (0) and sorted by deletion size. WT reads, tins, 1 bp insertions, insertions, and delins are color coded. The degree of blue coloring reflects the extent of microhomology used for deletion formation.

(B) Quantification of sequence products obtained from indicated cell lines treated with ART558 and NU7441 as indicated and transfected with Cas9-WT and sgHPRT_Ex3.2 (left panel) or sgHPRT_Ex4 (right panel). Unselected cells were collected for DNA extraction and used for short-read (∼200 bp) targeted sequencing around the break site. Data are represented as average (n = 2) ± SD.

(C) Quantification of a specific microhomology-driven 6 bp deletion from indicated cell lines treated with ART558 and NU7441 as indicated and transfected with Cas9-WT and sgHPRT_Ex4. Data are represented as average (n = 2) ± SEM.

cells to identify DSB sequence contexts that preferentially produce mutational outcomes that best typify either NHEJ or TMEJ. Based on the tornado plots displayed in Figure 3A, we chose sgRNA_ex3.2 and sgRNA_ex4 to this end: the 1 bp insertion that is dominating the spectrum of sgRNA_ex3.2 is a typical NHEJ product, whereas the 6 bp deletion with 4 bp of microhomology at its junction, which is prominently present in sgRNA_ex4, represents TMEJ activity. Subsequently, we established repair profiles for four different somatic human cell lines that are commonly used in research (HEK293T, HeLa, U2OS, and RPE1). Cells were transfected with CRISPR reagents and cultured in medium either without or supplemented with TMEJ-inhibitor ART558, NHEJ-inhibitor NU7741, or both inhibitors. Seven days post-transfection, DNA was isolated and used for targeted sequencing. Despite a high transfection efficiency for all cell lines, the targeting efficiency in RPE1 cells was relatively low (Figure S3A), possibly because of a proficient p53-mediated

DNA damage response to Cas9-induced DSBs.[39] The other three cell lines revealed a significant induction of mutations at both *HPRT* target sites (Figure 3B). Mutational signature analysis revealed that the EJ-pathway-specific inhibitors profoundly affect the types of mutations that are induced by CRISPR-Cas9 targeting. For all cell lines tested, the NHEJ-dependent 1 bp insertions prevalent on target site HPRT_ex3.2 are suppressed by NU7441 but not by ART558. The majority of mutational outcomes in these NHEJ-inhibited conditions are products of TMEJ, as additional inhibition of PolΘ by ART558 in those cells leads to a profound reduction in the total number of altered alleles (Figures 3B, S3A, and S3B). While TMEJ becomes more prominent upon NHEJ inhibition, the opposite is also evident: prevalent microhomology-mediated deletions at target site HPRT_ex4 are suppressed by ART558 but are increased upon NHEJ inhibition (Figure 3C). Also at this site, and for the three human cell lines tested, the overall frequency of mutations is
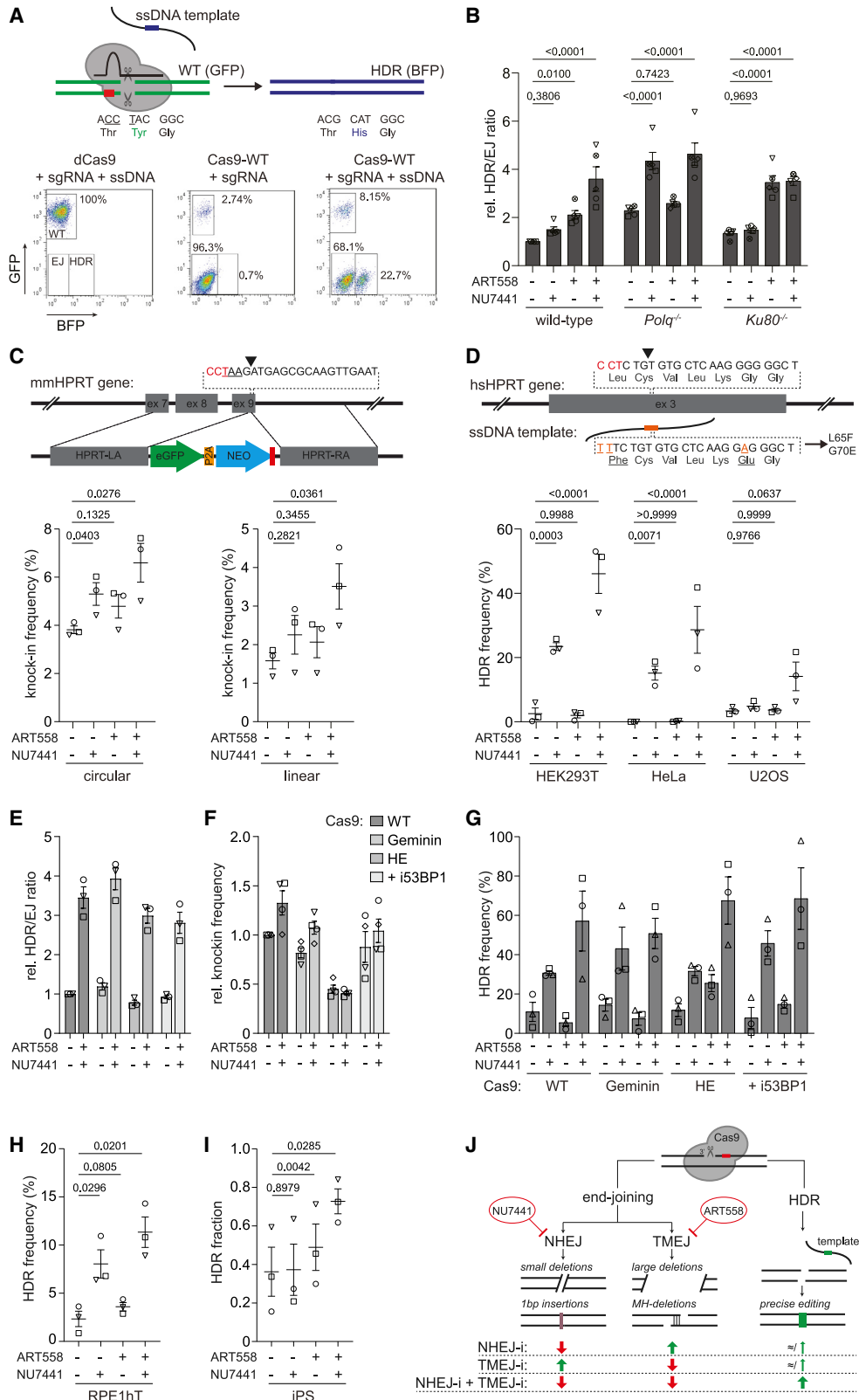
(legend on next page)

reduced by simultaneous inhibition of NHEJ and TMEJ (Figure 3B). Finally, we monitored the effect of ART558 on target site HPRT_ex7, which has a more homogenous mutational signature (Figure 3A) lacking clear telltale outcomes for both EJ pathways. Here, the TMEJ-inhibiting effect of ART558 treatment is less prominent but still evident (most notably in U2OS cells): a reduction in the degree of microhomology at deletion junctions and a decrease in the number of templated insertions (Figures S3C and S3D). We conclude that CRISPR-Cas9-mediated genome editing can be directed toward a preferential outcome not only by the choice of target sequence but also by pharmacological inhibition of mutagenic DSB repair.

PolΘ (co-)inhibition promotes HDR at CRISPR-Cas9-induced breaks

We next wished to test whether suppression of mutagenic repair at CRISPR-Cas9-induced breaks by ART558 (and NU7441) impacts precise gene editing through HDR. To this end, we generated wild-type, $Polq^{-/-}$, and $Ku80^{-/-}$ mESC lines containing stably integrated monoallelic GFP at the Rosa26 locus (Figures S4A and S4B). GFP can be converted to BFP by a tyrosine to histidine substitution at residue 66. We used this assay to monitor HDR of a Cas9-induced DSB that uses a co-transfected single strand DNA (ssDNA) donor that harbors three nucleotide variants as a repair template, which converts GFP to BFP; the resulting shift in the fluorescence excitation and emission spectra can be used as a proxy for CRISPR-Cas9-mediated gene editing (Figure 4A).[21,40] We next measured the levels of BFP+ (HDR) and

non-fluorescent (EJ) cells upon delivery of sgRNA/Cas9 plasmid and ssDNA template in cells of different genotype treated either with ART558, with DNA-PK inhibitor NU7441, or with a combination of both. On average, we observed a ~2-fold increase in the HDR/EJ ratio upon inhibition of PolΘ with ART558 in wild-type cells, an effect that could be further enhanced when combined with NU7441 (Figures 4B and S4C). Control experiments in PolΘ- and Ku80-deficient cells again demonstrates the specificity of both EJ inhibitors: only NU7441 has an additive effect on the HDR/EJ ratio in $Polq^{-/-}$ cells, while only ART558 treatment increases this ratio in $Ku80^{-/-}$ cells (Figure 4B). Interestingly, PolΘ inhibition either by ART558 treatment or in $Polq^{-/-}$ knockout cells has the strongest effect on HDR; co-treatment with DNA-PK inhibitor increases the HDR/EJ ratio primarily by lowering the EJ fraction, which we verified by targeted sequencing of the GFP target site (Figures S4C and S4D).

We next investigated the effect of combined EJ inhibition on the efficiency of CRISPR-Cas9-mediated targeted knockin of foreign DNA. To this end, we used an sgRNA targeting the mouse HPRT stop codon and a plasmid containing an EGFP-P2A-Neomycin construct flanked by 1 kb HPRT homology arms (Figure 4C). Introducing these reagents into mESCs results in detectable HPRT-EGFP expression exclusively in cells co-expressing Cas9-wild type (WT) (Figure S4E) and can thus be used to measure the frequency of knockin cells. Using both circular as well as linearized dsDNA donor templates, we found that ART558 or NU7441 single treatment increases the knockin frequency, an effect that could be further enhanced by combining both EJ

Figure 4. ART558 and NU7441 treatment promotes homology-driven repair (HDR) at CRISPR-Cas9-induced breaks

(A) Top panel: schematic representation of the GFP to BFP conversion assay. Sequences and encoded amino acids of the unedited EGFP (WT) and edited BFP (HDR) loci are presented, and the used PAM site in EGFP is underlined. Bottom panel: representative GFP-BFP flow cytometry scatter plots of GFP-Rosa reporter cells transfected with an EGFP sgRNA and either nuclease dead Cas9 (dCas9) and ssDNA template (left panel), Cas9-WT without template (middle panel), or Cas9-WT and ssDNA template (right panel). Gated populations are GFP$^+$ (WT, unedited), GFP$^-$ (end joining [EJ]), and BFP$^+$ (HDR).

(B) Relative HDR/EJ ratio determined by flow cytometry in the indicated GFP-Rosa mESC lines treated with indicated inhibitors and transfected with an EGFP sgRNA, Cas9-WT, and ssDNA template. The data shown represent the mean ± SEM (n = 5, indicated by different symbols) and are expressed as a fraction of the HDR/EJ ratio observed in untreated WT cells (set to 1).

(C) Top panel: schematic representation of the HPRT-EGFP knockin strategy. The HPRT gene, the sgRNA (sequence inset), and the PAM site (red) used to target the stop codon (underlined sequence) and the EGFP-P2A-NEO targeting construct with ~1 kb HPRT homology arms are represented. Bottom panel: quantification of the HPRT-EGFP knockin frequency determined by flow cytometry in WT mESCs treated with indicated inhibitors and transfected with the HPRT sgRNA, Cas9-WT, and either circular (left) or linear (right) EGFP-P2A-NEO targeting construct. The mean ± SEM is indicated (n = 3, indicated by different symbols). Statistical significance was calculated via unpaired t test.

(D) Top panel: schematic representation of the HDR assay at the human HPRT gene. The human HPRT gene, the sgRNA (top sequence inset), and the PAM site (red) used to target HPRT exon 3, as well as the ssDNA template (bottom sequence inset) used to introduce the L65F and G70E variants (orange, underlined) are represented. Bottom panel: quantification of HDR frequency as determined by TIDER in HEK293T, HeLa, or U2OS cells treated with indicated inhibitors and transfected with the HPRT sgRNA, Cas9-WT, and ssDNA template. The mean ± SEM is indicated (n = 3, indicated by different symbols).

(E) Relative HDR/EJ ratio determined by flow cytometry in WT GFP-Rosa mESC lines treated with indicated inhibitors and transfected with an EGFP sgRNA and a ssDNA template together with either Cas9 only (WT), Cas9-Geminin, Cas9-HE, or Cas9 co-expressing i53BP1. The data shown represent the mean ± SEM (n = 3, indicated by different symbols) and are expressed as a fraction of the HDR/EJ ratio observed in untreated cells transfected with Cas9 (set to 1).

(F) Quantification of the HPRT-EGFP knockin frequency determined by flow cytometry in WT mESCs treated with indicated inhibitors and transfected with the HPRT sgRNA, different Cas9 variants as described in (E), and circular EGFP-P2A-NEO targeting construct. The mean ± SEM is indicated (n = 3, indicated by different symbols).

(G) Quantification of HDR frequency as determined by TIDER in HEK293T cells treated with indicated inhibitors and transfected with the HPRT sgRNA, different Cas9 variants as described in (E), and ssDNA template. The mean ± SEM is indicated (n = 3, indicated by different symbols).

(H) Quantification of HDR frequency as determined by targeted sequencing in RPE1hT cells treated with indicated inhibitors and transfected with the HPRT sgRNA, Cas9-WT, and ssDNA template. The mean ± SEM is indicated (n = 3, indicated by different symbols).

(I) Quantification of HDR fraction as determined by targeted sequencing in human iPSCs treated with indicated inhibitors and transduced with an EGFP sgRNA, Cas9-WT, and ssDNA template. The mean ± SEM is indicated (n = 3, indicated by different symbols).

(J) Scheme representing different repair outcomes of Cas9-induced breaks; green and red arrows indicate how to modulate these outcomes using EJ inhibitors (i). Statistical significance in (B) and (D) was calculated via two-way ANOVA multiple comparisons with Dunnett's test, comparing means of treated cells with the mean of untreated (DMSO) cells. Statistical significance in (E) and (F) was calculated via paired t test. p values are indicated in the figure panels.

inhibitors (Figure 4C). Thus, transient inhibition of NHEJ and TMEJ can be used to improve the frequency of targeted integration of foreign DNA into defined loci. To substantiate the potential usage of ART558 to increase the desired high-fidelity outcome for gene editing, we performed CRISPR-Cas9 HDR experiments in human cell lines. As a target test case, we used an ssDNA template to introduce two pathogenic variants (L65F and G70E, ClinVar database[41]) in *HPRT* (Figure 4D). Seven days after transfecting HEK293T, HeLa, and U2OS cells with Cas9-WT, an sgRNA targeting *HPRT* exon 3, and an ssDNA repair template containing the desired mutations, we isolated DNA from cells and performed PCRs on the targeted region. Sanger sequencing of the amplicons was performed, and TIDER software was used to deconvolute indel and HDR frequencies.[42] We found that ART558 treatment by itself does not alter the relatively low HDR frequency found for these cell types. NU7441 treatment increases the fraction of specific gene edits in HEK293T and HeLa cells but not in U2OS cells. The notion that NU7441 treatment suppresses the formation of 1 bp insertions while increasing the ratio of deletions suggests that more prominent TMEJ activity under these conditions may limit precise gene editing. Indeed, treating cells with both NU7441 and ART558 resulted in a profound increase in the frequency of HDR (Figures 4D and S4F). We next wished to compare the use of the two EJ pathway inhibitors to several other strategies previously reported to improve HDR at CRISPR-Cas9-induced breaks.[22,24,43] To our surprise, we observed little to no additive effect of these other strategies on HDR levels using either ssDNA or dsDNA in combination with the NU7441 + ART558 cocktail (Figures 4E and 4F) in mESCs. Potential differences between mouse and human were addressed by including human HEK293 cells and found for these cells that certain Cas9 fusions, but only in combination with one of both inhibitors, had a small additional effect on HDR frequency (e.g., Cas9-HE with ART558; Figure 4G). In addition, prolonging the S phase using the CDC7 inhibitor XL413 mildly increased HDR frequency when used in combination with the EJ inhibitors (Figure S4G).[44] Finally, we wanted to test the effect of using combined EJ inhibition on HDR frequency in non-cancerous and more clinically relevant human cells. To this end, we used the near-diploid, karyotype-stable RPE1 cell line and assayed the effect of EJ inhibition on HDR. Indeed, also these cells are susceptible to gene targeting enhancement by using combined inhibition of NHEJ and TMEJ (Figure 4H). In addition, we transduced GFP+ human induced pluripotent stem cells (iPSCs) with Cas9, an sgRNA targeting GFP and a ssDNA donor template harboring three nucleotide variants. Targeted sequencing of the break site to inspect for precise gene editing revealed that the combined usage of NU7441 and ART558 outperformed conditions where only one of inhibitors was used (Figure 4I).

Together, our data shows that precise gene editing can be accomplished at high frequencies via transient pharmacological inhibition of both mutagenic EJ pathways (Figure 4J).

DISCUSSION

Targeting Polθ has been recognized as a potentially promising treatment strategy for tumors deficient in homologous recombination (HR) repair[34] as HR-deficient cells are critically reliant on TMEJ

to repair DSBs. Inhibition of Polθ can therefore be exploited to induce synthetic lethality in tumor cells specifically.[45] This notion led to several initiatives to find clinically viable chemical inhibitors of Polθ; ART558 was recently developed as a potent and specific small-molecule inhibitor of Polθ. Here, we demonstrate that ART558 can also be useful in genome-editing applications. We demonstrate that Polθ inhibition stimulates HDR at CRISPR-Cas9-induced breaks through attenuating mutagenic EJ. In addition, it was recently shown that Polθ (and Nbs1) induces large deletions at CRISPR-Cas9-induced breaks[37]; here, we present an easy and robust way to prevent such undesired outcomes by adding ART558 to editing experiments. This suppressive effect is important as the incidence of large deletions has frequently been underestimated because of the loss of sequences to which PCR primers are designed in diagnostic approaches, leading to misinterpretation of both knockout and knockin alleles.[10,46] Besides promoting HDR and suppressing large deletions, ART558 may also be used to favor NHEJ as a repair outcome at target sites where small indel formation upon CRISPR-Cas9 is potentially therapeutic[47–50]: for example, 1 bp insertions, which are a more prominent outcome in ART558-treated cells, have recently been show to restore dystrophin expression in *in vivo* models of Duchenne muscular dystrophy.[51,52] Favoring 1 bp insertions over potential in-frame microhomology-mediated deletions will also increase the efficiency of generating knockout alleles.[50]

The notion that TMEJ is a more prominent contributor to the mutation profile in mESCs versus human cancer cell lines may suggest that inhibition of Polθ is most impactful in cells with a high proliferation index, which fits with prominent TMEJ action in embryonic and germ cells in several species.[26,29,30] In addition, recent work demonstrated that TMEJ of spontaneous breaks in HR-deficient cells is delayed until mitosis,[53] and it is therefore likely that the efficacy of ART558 in CRISPR-Cas9 experiments will be cell-type dependent. In line with our findings, large-scale analysis of Cas9-induced mutational signatures revealed that somatic cells often favor 1 bp insertions, while human iPSCs and mESCs showed higher rates of microhomology-mediated deletions, suggestive of increased TMEJ activity in pluripotent stem cells.[54] Presumably, fast replicating cells more often encounter breaks that are incompatible with NHEJ and HR and thus require TMEJ for repair.[55] We envisage two related scenarios: (1) since HR cannot occur without an intact template, DSBs introduced in both sister chromatids by efficient CRISPR-Cas9 activity will be forced to repair by alternative means, i.e., TMEJ, and (2) replication through an unrepaired CRISPR-induced break will create a similar situation, with DSBs refractory to HR and reliant on repair by TMEJ.[56] Such DSBs will be more frequently induced by CRISPR in WT cells in S/G2. Conversely, in somatic cells that spend more time in G1 phase, Cas9-mediated breaks are more often introduced pre-replication, where they can be efficiently repaired by NHEJ. In these cells, TMEJ may become prevalent upon perturbation of NHEJ, presumably acting on replication-associated breaks resulting from unresolved (Cas9-induced) damage in G1.[27,57–60] Hence, inhibition of NHEJ alone could lead to increased TMEJ activity; indeed, a profound shift toward microhomology-mediated deletions is observed at CRISPR-Cas9-induced breaks in somatic cells upon the inhibition of DNA-PK.[61]

In summary, we show here the ability to change the mutational outcome of CRISPR-Cas9 editing by using small-molecule inhibitors, which temporally interfere with a cell's capacity to employ specific DNA repair enzymes. In addition, we demonstrate that combining pathway-specific inhibitors leads to profoundly increased efficiencies of HDR-mediated repair at CRISPR-Cas9-induced breaks, going from marginal levels to 30%–50% in several human cell lines (Figure 4D). Importantly, even small increases in HDR could make a substantial therapeutic difference, for example in monogenic disorders where corrected cells have an increased fitness and thus a selective advantage compared with non-corrected cells (e.g., in SCID-X1 and certain patients with Fanconi anemia).[62–64] We foresee that the ability to direct the outcome of CRISPR-Cas9 toward a desired mutation and to achieve higher levels of precise editing while suppressing adverse effects will facilitate the development of improved tools for basic research and may also accelerate the development of safer CRISPR-based therapies for the benefit of human health.

Limitations of the study

Here, we have studied the effect of EJ inhibitors on the outcome of CRISPR-Cas9-induced break repair but have used PCR-based assays that restrict the types of outcomes to deletions of a given size, i.e., smaller than ∼3.5 kb. While we show the number of kb-sized deletions to be reduced upon TMEJ inhibition, we have not determined the potential effect on even larger deletions and other chromosomal rearrangements (e.g., translocations) that have been reported at CRISPR-Cas9 on- and off-target sites.[6,8] We thus provide no quantitative inventory of all potential genome alterations. Sequencing of off-target cleavage sites through dsDNA capturing methods (e.g., GUIDE-seq[6]) and/or whole-genome sequencing of CRISPR-Cas9-targeted cell-lines can be used to determine the full effect of EJ inhibitors on the entire spectra of mutations.

Another limitation is the limited number of genomic sites that we targeted and that we used optimal parameters in our targeting experiments: a short "cut-to-editing" distance was chosen, and we introduced mutations in the sgRNA and/or PAM to prevent re-cutting. How the dual EJ inhibition strategy performs on target sites where these options are limited remains to be determined. Finally, it may be worthwhile to recite here that we have used a limited set of cell lines, all of which were selected because of useful growth characteristics in cell culture. Clinical usage of CRISPR technologies may be directed at cell types (e.g., neuronal cells) for which we at this moment have not established the relative contribution of the different repair pathways.

STAR★METHODS

Detailed methods are provided in the online version of this paper and include the following:

- KEY RESOURCES TABLE
- RESOURCE AVAILABILITY
  - ○ Lead contact
  - ○ Materials availability
  - ○ Data and code availability
- EXPERIMENTAL MODEL AND SUBJECT DETAILS

  - ○ Cell culture and cell lines
- METHOD DETAILS
  - ○ Chemicals
  - ○ Plasmids
  - ○ Transfections
  - ○ *HPRT-eGFP* gene mutation assay
  - ○ Targeted sequencing of Cas9-induced repair outcomes
  - ○ Sequence analysis Cas9-induced repair outcomes
  - ○ HDR experiments mES cells
  - ○ HDR experiment human cells and TIDER analysis
- QUANTIFICATION AND STATISTICAL ANALYSIS

REFERENCES

1. van Schendel, R., Schimmel, J., and Tijsterman, M. (2022). SIQ: easy quantitative measurement of mutation profiles in sequencing data. NAR Genom. Bioinform. *4*, lqac063. https://doi.org/10.1093/nargab/lqac063.

2. Jinek, M., Chylinski, K., Fonfara, I., Hauer, M., Doudna, J.A., and Charpentier, E. (2012). A programmable dual-RNA-guided DNA endonuclease

in adaptive bacterial immunity. Science *337*, 816–821. https://doi.org/10.1126/science.816.

3. Ran, F.A., Hsu, P.D., Wright, J., Agarwala, V., Scott, D.A., and Zhang, F. (2013). Genome engineering using the CRISPR-Cas9 system. Nat. Protoc. *8*, 2281–2308. https://doi.org/10.1038/nprot.2013.143.

4. Cong, L., Ran, F.A., Cox, D., Lin, S., Barretto, R., Habib, N., Hsu, P.D., Wu, X., Jiang, W., Marraffini, L.A., and Zhang, F. (2013). Multiplex genome engineering using CRISPR/Cas systems. Science *339*, 819–823. https://doi.org/10.1126/science.819.

5. Mali, P., Yang, L., Esvelt, K.M., Aach, J., Guell, M., DiCarlo, J.E., Norville, J.E., and Church, G.M. (2013). RNA-guided human genome engineering via Cas9. Science *339*, 823–826. https://doi.org/10.1126/science.823.

6. Tsai, S.Q., Zheng, Z., Nguyen, N.T., Liebers, M., Topkar, V.V., Thapar, V., Wyvekens, N., Khayter, C., Iafrate, A.J., Le, L.P., et al. (2015). GUIDE-seq enables genome-wide profiling of off-target cleavage by CRISPR-Cas nucleases. Nat. Biotechnol. *33*, 187–197. https://doi.org/10.1038/nbt.3117.

7. Hanlon, K.S., Kleinstiver, B.P., Garcia, S.P., Zaborowski, M.P., Volak, A., Spirig, S.E., Muller, A., Sousa, A.A., Tsai, S.Q., Bengtsson, N.E., et al. (2019). High levels of AAV vector integration into CRISPR-induced DNA breaks. Nat. Commun. *10*, 4439. https://doi.org/10.1038/s41467-019-12449-2.

8. Cullot, G., Boutin, J., Toutain, J., Prat, F., Pennamen, P., Rooryck, C., Teichmann, M., Rousseau, E., Lamrissi-Garcia, I., Guyonnet-Duperat, V., et al. (2019). CRISPR-Cas9 genome editing induces megabase-scale chromosomal truncations. Nat. Commun. *10*, 1136. https://doi.org/10.1038/s41467-019-09006-2.

9. Ma, H., Marti-Gutierrez, N., Park, S.W., Wu, J., Lee, Y., Suzuki, K., Koski, A., Ji, D., Hayama, T., Ahmed, R., et al. (2017). Correction of a pathogenic gene mutation in human embryos. Nature *548*, 413–419. https://doi.org/10.1038/nature23305.

10. Adikusuma, F., Piltz, S., Corbett, M.A., Turvey, M., McColl, S.R., Helbig, K.J., Beard, M.R., Hughes, J., Pomerantz, R.T., and Thomas, P.Q. (2018). Large deletions induced by Cas9 cleavage. Nature *560*, E8–E9. https://doi.org/10.1038/s41586-018-0380-z.

11. Kosicki, M., Tomberg, K., and Bradley, A. (2018). Repair of double-strand breaks induced by CRISPR-Cas9 leads to large deletions and complex rearrangements. Nat. Biotechnol. *36*, 765–771. https://doi.org/10.1038/nbt.4192.

12. Owens, D.D.G., Caulder, A., Frontera, V., Harman, J.R., Allan, A.J., Bucakci, A., Greder, L., Codner, G.F., Hublitz, P., McHugh, P.J., et al. (2019). Microhomologies are prevalent at Cas9-induced larger deletions. Nucleic Acids Res. *47*, 7402–7417. https://doi.org/10.1093/nar/gkz459.

13. Alanis-Lobato, G., Zohren, J., McCarthy, A., Fogarty, N.M.E., Kubikova, N., Hardman, E., Greco, M., Wells, D., Turner, J.M.A., and Niakan, K.K. (2021). Frequent loss of heterozygosity in CRISPR-Cas9-edited early human embryos. Proc. Natl. Acad. Sci. USA *118*, e2004832117. https://doi.org/10.1073/pnas.2004832117.

14. Gaudelli, N.M., Komor, A.C., Rees, H.A., Packer, M.S., Badran, A.H., Bryson, D.I., and Liu, D.R. (2017). Programmable base editing of A*T to G*C in genomic DNA without DNA cleavage. Nature *551*, 464–471. https://doi.org/10.1038/nature24644.

15. Komor, A.C., Kim, Y.B., Packer, M.S., Zuris, J.A., and Liu, D.R. (2016). Programmable editing of a target base in genomic DNA without double-stranded DNA cleavage. Nature *533*, 420–424. https://doi.org/10.1038/nature17946.

16. Chen, X., Janssen, J.M., Liu, J., Maggio, I., t Jong, A.E.J., Mikkers, H.M.M., and Gonçalves, M.A.F.V. (2017). In trans paired nicking triggers seamless genome editing without double-stranded DNA cutting. Nat. Commun. *8*, 657. https://doi.org/10.1038/s41467-017-00687-1.

17. Anzalone, A.V., Randolph, P.B., Davis, J.R., Sousa, A.A., Koblan, L.W., Levy, J.M., Chen, P.J., Wilson, C., Newby, G.A., Raguram, A., and Liu, D.R. (2019). Search-and-replace genome editing without double-strand breaks or donor DNA. Nature *576*, 149–157. https://doi.org/10.1038/s41586-019-1711-4.

18. Chen, P.J., Hussmann, J.A., Yan, J., Knipping, F., Ravisankar, P., Chen, P.F., Chen, C., Nelson, J.W., Newby, G.A., Sahin, M., et al. (2021). Enhanced prime editing systems by manipulating cellular determinants of editing outcomes. Cell *184*, 5635–5652.e29. https://doi.org/10.1016/j.cell.2021.09.018.

19. Schene, I.F., Joore, I.P., Oka, R., Mokry, M., van Vugt, A.H.M., van Boxtel, R., van der Doef, H.P.J., van der Laan, L.J.W., Verstegen, M.M.A., van Hasselt, P.M., et al. (2020). Prime editing for functional repair in patient-derived disease models. Nat. Commun. *11*, 5352. https://doi.org/10.1038/s41467-020-19136-7.

20. Anzalone, A.V., Koblan, L.W., and Liu, D.R. (2020). Genome editing with CRISPR-Cas nucleases, base editors, transposases and prime editors. Nat. Biotechnol. *38*, 824–844. https://doi.org/10.1038/s41587-020-0561-9.

21. Richardson, C.D., Ray, G.J., DeWitt, M.A., Curie, G.L., and Corn, J.E. (2016). Enhancing homology-directed genome editing by catalytically active and inactive CRISPR-Cas9 using asymmetric donor DNA. Nat. Biotechnol. *34*, 339–344. https://doi.org/10.1038/nbt.3481.

22. Charpentier, M., Khedher, A.H.Y., Menoret, S., Brion, A., Lamribet, K., Dardillac, E., Boix, C., Perrouault, L., Tesson, L., Geny, S., et al. (2018). CtIP fusion to Cas9 enhances transgene integration by homology-dependent repair. Nat. Commun. *9*, 1133. https://doi.org/10.1038/s41467-018-03475-7.

23. Lin, S., Staahl, B.T., Alla, R.K., and Doudna, J.A. (2014). Enhanced homology-directed human genome engineering by controlled timing of CRISPR/Cas9 delivery. Elife *3*, e04766. https://doi.org/10.7554/eLife.04766.

24. Gutschner, T., Haemmerle, M., Genovese, G., Draetta, G.F., and Chin, L. (2016). Post-translational regulation of Cas9 during G1 enhances homology-directed repair. Cell Rep. *14*, 1555–1566. https://doi.org/10.1016/j.celrep.2016.01.019.

25. Yeh, C.D., Richardson, C.D., and Corn, J.E. (2019). Advances in genome editing through control of DNA repair pathways. Nat. Cell Biol. *21*, 1468–1478. https://doi.org/10.1038/s41556-019-0425-z.

26. Schimmel, J., Kool, H., van Schendel, R., and Tijsterman, M. (2017). Mutational signatures of non-homologous and polymerase theta-mediated end-joining in embryonic stem cells. EMBO J. *36*, 3634–3649. https://doi.org/10.15252/embj.201796948.

27. Wyatt, D.W., Feng, W., Conlin, M.P., Yousefzadeh, M.J., Roberts, S.A., Mieczkowski, P., Wood, R.D., Gupta, G.P., and Ramsden, D.A. (2016). Essential roles for polymerase theta-mediated end joining in the repair of chromosome breaks. Mol. Cell *63*, 662–673. https://doi.org/10.1016/j.molcel.2016.06.020.

28. Hussmann, J.A., Ling, J., Ravisankar, P., Yan, J., Cirincione, A., Xu, A., Simpson, D., Yang, D., Bothmer, A., Cotta-Ramusino, C., et al. (2021). Mapping the genetic landscape of DNA double-strand break repair. Cell *184*, 5653–5669.e25. https://doi.org/10.1016/j.cell.2021.10.002.

29. Thyme, S.B., and Schier, A.F. (2016). Polq-mediated end joining is essential for surviving DNA double-strand breaks during early zebrafish development. Cell Rep. *15*, 707–714. https://doi.org/10.1016/j.celrep.2016.03.072.

30. van Schendel, R., Roerink, S.F., Portegijs, V., van den Heuvel, S., and Tijsterman, M. (2015). Polymerase Theta is a key driver of genome evolution and of CRISPR/Cas9-mediated mutagenesis. Nat. Commun. *6*, 7394. https://doi.org/10.1038/ncomms8394.

31. Carvajal-Garcia, J., Cho, J.E., Carvajal-Garcia, P., Feng, W., Wood, R.D., Sekelsky, J., Gupta, G.P., Roberts, S.A., and Ramsden, D.A. (2020). Mechanistic basis for microhomology identification and genome scarring by polymerase theta. Proc. Natl. Acad. Sci. USA *117*, 8476–8485. https://doi.org/10.1073/pnas.1921791117.

32. Arai, D., and Nakao, Y. (2021). Efficient biallelic knock-in in mouse embryonic stem cells by in vivo-linearization of donor and transient inhibition of DNA polymerase theta/DNA-PK. Sci. Rep. *11*, 18132. https://doi.org/10.1038/s41598-021-97579-8.

33. Mateos-Gomez, P.A., Kent, T., Deng, S.K., McDevitt, S., Kashkina, E., Hoang, T.M., Pomerantz, R.T., and Sfeir, A. (2017). The helicase domain

of Poltheta counteracts RPA to promote alt-NHEJ. Nat. Struct. Mol. Biol. *24*, 1116–1123. https://doi.org/10.1038/nsmb.3494.

34. Zatreanu, D., Robinson, H.M.R., Alkhatib, O., Boursier, M., Finch, H., Geo, L., Grande, D., Grinkevich, V., Heald, R.A., Langdon, S., et al. (2021). Poltheta inhibitors elicit BRCA-gene synthetic lethality and target PARP inhibitor resistance. Nat. Commun. *12*, 3636. https://doi.org/10.1038/s41467-021-23463-8.

35. Stockley, M.L., Ferdinand, A., Benedetti, G., Blencowe, P., Boyd, S.M., Calder, M., Charles, M.D., Edwardes, L.V., Ekwuru, T., Finch, H., et al. (2022). Discovery, characterization, and structure-based optimization of small-molecule in vitro and in vivo probes for human DNA polymerase theta. J. Med. Chem. *65*, 13879–13891. https://doi.org/10.1021/acs.jmedchem.2c01142.

36. Schimmel, J., Muñoz-Subirana, N., Kool, H., van Schendel, R., and Tijsterman, M. (2021). Small tandem DNA duplications result from CST-guided Pol alpha-primase action at DNA break termini. Nat. Commun. *12*, 4843. https://doi.org/10.1038/s41467-021-25154-w.

37. Kosicki, M., Allen, F., Steward, F., Tomberg, K., Pan, Y., and Bradley, A. (2022). Cas9-induced large deletions and small indels are controlled in a convergent fashion. Nat. Commun. *13*, 3422. https://doi.org/10.1038/s41467-022-30480-8.

38. McInnes, L., Healy, J., and Melville, J. (2018). UMAP: Uniform Manifold approximation and projection for dimension reduction. Preprint at arXiv. https://doi.org/10.48550/arXiv.1802.03426.

39. Haapaniemi, E., Botla, S., Persson, J., Schmierer, B., and Taipale, J. (2018). CRISPR-Cas9 genome editing induces a p53-mediated DNA damage response. Nat. Med. *24*, 927–930. https://doi.org/10.1038/s41591-018-0049-z.

40. Glaser, A., McColl, B., and Vadolas, J. (2016). GFP to BFP conversion: a versatile assay for the quantification of CRISPR/cas9-mediated genome editing. Mol. Ther. Nucleic Acids *5*, e334. https://doi.org/10.1038/mtna.2016.48.

41. Landrum, M.J., Lee, J.M., Riley, G.R., Jang, W., Rubinstein, W.S., Church, D.M., and Maglott, D.R. (2014). ClinVar: public archive of relationships among sequence variation and human phenotype. Nucleic Acids Res. *42*, D980–D985. https://doi.org/10.1093/nar/gkt1113.

42. Brinkman, E.K., Kousholt, A.N., Harmsen, T., Leemans, C., Chen, T., Jonkers, J., and van Steensel, B. (2018). Easy quantification of template-directed CRISPR/Cas9 editing. Nucleic Acids Res. *46*, e58. https://doi.org/10.1093/nar/gky164.

43. Canny, M.D., Moatti, N., Wan, L.C.K., Fradet-Turcotte, A., Krasner, D., Mateos-Gomez, P.A., Zimmermann, M., Orthwein, A., Juang, Y.C., Zhang, W., et al. (2018). Inhibition of 53BP1 favors homology-dependent DNA repair and increases CRISPR-Cas9 genome-editing efficiency. Nat. Biotechnol. *36*, 95–102. https://doi.org/10.1038/nbt.4021.

44. Wienert, B., Nguyen, D.N., Guenther, A., Feng, S.J., Locke, M.N., Wyman, S.K., Shin, J., Kazane, K.R., Gregory, G.L., Carter, M.A.M., et al. (2020). Timed inhibition of CDC7 increases CRISPR-Cas9 mediated templated repair. Nat. Commun. *11*, 2109. https://doi.org/10.1038/s41467-020-15845-1.

45. Ramsden, D.A., Carvajal-Garcia, J., and Gupta, G.P. (2022). Mechanism, cellular functions and cancer roles of polymerase-theta-mediated DNA end joining. Nat. Rev. Mol. Cell Biol. *23*, 125–140. https://doi.org/10.1038/s41580-021-00405-2.

46. Shin, H.Y., Wang, C., Lee, H.K., Yoo, K.H., Zeng, X., Kuhns, T., Yang, C.M., Mohr, T., Liu, C., and Hennighausen, L. (2017). CRISPR/Cas9 targeting events cause complex deletions and insertions at 17 sites in the mouse genome. Nat. Commun. *8*, 15464. https://doi.org/10.1038/ncomms15464.

47. Román-Rodríguez, F.J., Ugalde, L., Álvarez, L., Díez, B., Ramírez, M.J., Risueño, C., Cortón, M., Bogliolo, M., Bernal, S., March, F., et al. (2019). NHEJ-mediated repair of CRISPR-cas9-induced DNA breaks efficiently corrects mutations in HSPCs from patients with Fanconi anemia. Cell Stem Cell *25*, 607–621.e7. https://doi.org/10.1016/j.stem.2019.08.016.

48. Wu, Y., Zeng, J., Roscoe, B.P., Liu, P., Yao, Q., Lazzarotto, C.R., Clement, K., Cole, M.A., Luk, K., Baricordi, C., et al. (2019). Highly efficient therapeutic gene editing of human hematopoietic stem cells. Nat. Med. *25*, 776–783. https://doi.org/10.1038/s41591-019-0401-y.

49. Olson, E.N. (2021). Toward the correction of muscular dystrophy by gene editing. Proc. Natl. Acad. Sci. USA *118*, e2004840117. https://doi.org/10.1073/pnas.2004840117.

50. Bermudez-Cabrera, H.C., Culbertson, S., Barkal, S., Holmes, B., Shen, M.W., Zhang, S., Gifford, D.K., and Sherwood, R.I. (2021). Small molecule inhibition of ATM kinase increases CRISPR-Cas9 1-bp insertion frequency. Nat. Commun. *12*, 5111. https://doi.org/10.1038/s41467-021-25415-8.

51. Amoasii, L., Hildyard, J.C.W., Li, H., Sanchez-Ortiz, E., Mireault, A., Caballero, D., Harron, R., Stathopoulou, T.R., Massey, C., Shelton, J.M., et al. (2018). Gene editing restores dystrophin expression in a canine model of Duchenne muscular dystrophy. Science *362*, 86–91. https://doi.org/10.1126/science.aau1549.

52. Amoasii, L., Long, C., Li, H., Mireault, A.A., Shelton, J.M., Sanchez-Ortiz, E., McAnally, J.R., Bhattacharyya, S., Schmidt, F., Grimm, D., et al. (2017). Single-cut genome editing restores dystrophin expression in a new mouse model of muscular dystrophy. Sci. Transl. Med. *9*, eaan8081. https://doi.org/10.1126/scitranslmed.aan8081.

53. Llorens-Agost, M., Ensminger, M., Le, H.P., Gawai, A., Liu, J., Cruz-García, A., Bhetawal, S., Wood, R.D., Heyer, W.D., and Löbrich, M. (2021). POLtheta-mediated end joining is restricted by RAD52 and BRCA2 until the onset of mitosis. Nat. Cell Biol. *23*, 1095–1104. https://doi.org/10.1038/s41556-021-00764-0.

54. Allen, F., Crepaldi, L., Alsinet, C., Strong, A.J., Kleshchevnikov, V., De Angeli, P., Páleníková, P., Khodak, A., Kiselev, V., Kosicki, M., et al. (2018). Predicting the mutations generated by repair of Cas9-induced double-strand breaks. Nat. Biotechnol. *37*, 64–72. https://doi.org/10.1038/nbt.4317.

55. Schimmel, J., van Schendel, R., den Dunnen, J.T., and Tijsterman, M. (2019). Templated insertions: a smoking gun for polymerase theta-mediated end joining. Trends Genet. *35*, 632–644. https://doi.org/10.1016/j.tig.2019.06.001.

56. Brinkman, E.K., Chen, T., de Haas, M., Holland, H.A., Akhtar, W., and van Steensel, B. (2018). Kinetics and fidelity of the repair of cas9-induced double-strand DNA breaks. Mol. Cell *70*, 801–813.e6. https://doi.org/10.1016/j.molcel.2018.04.016.

57. Koole, W., van Schendel, R., Karambelas, A.E., van Heteren, J.T., Okihara, K.L., and Tijsterman, M. (2014). A Polymerase Theta-dependent repair pathway suppresses extensive genomic instability at endogenous G4 DNA sites. Nat. Commun. *5*, 3216, [doi]. https://doi.org/10.1038/ncomms4216.

58. Roerink, S.F., van Schendel, R., and Tijsterman, M. (2014). Polymerase theta-mediated end joining of replication-associated DNA breaks in C. elegans. Genome Res. *24*, 954–962. https://doi.org/10.1101/gr.170431.113.

59. Wang, Z., Song, Y., Li, S., Kurian, S., Xiang, R., Chiba, T., and Wu, X. (2019). DNA Polymerase theta (POLQ) is important for repair of DNA double-strand breaks caused by fork collapse. J. Biol. Chem. *294*, 3909–3919. https://doi.org/10.1074/jbc.RA118.005188.

60. Yu, W., Lescale, C., Babin, L., Bedora-Faure, M., Lenden-Hasse, H., Baron, L., Demangel, C., Yelamos, J., Brunet, E., and Deriano, L. (2020). Repair of G1 induced DNA double-strand breaks in S-G2/M by alternative NHEJ. Nat. Commun. *11*, 5239. https://doi.org/10.1038/s41467-020-19060-w.

61. van Overbeek, M., Capurso, D., Carter, M.M., Thompson, M.S., Frias, E., Russ, C., Reece-Hoyes, J.S., Nye, C., Gradia, S., Vidal, B., et al. (2016). DNA repair profiling reveals nonrandom outcomes at cas9-mediated breaks. Mol. Cell *63*, 633–646. https://doi.org/10.1016/j.molcel.2016.06.037.

62. Cox, D.B.T., Platt, R.J., and Zhang, F. (2015). Therapeutic genome editing: prospects and challenges. Nat. Med. *21*, 121–131. https://doi.org/10.1038/nm.3793.

63. Gross, M., Hanenberg, H., Lobitz, S., Friedl, R., Herterich, S., Dietrich, R., Gruhn, B., Schindler, D., and Hoehn, H. (2002). Reverse mosaicism in Fanconi anemia: natural gene therapy via molecular self-correction. Cytogenet. Genome Res. *98*, 126–135. https://doi.org/10.1159/000069805.

64. Fischer, A., and Hacein-Bey-Abina, S. (2020). Gene therapy for severe combined immunodeficiencies and beyond. J. Exp. Med. *217*, e20190607. https://doi.org/10.1084/jem.20190607.

65. van de Kooij, B., Kruswick, A., van Attikum, H., and Yaffe, M.B. (2022). Multi-pathway DNA-repair reporters reveal competition between end-joining, single-strand annealing and homologous recombination at Cas9-induced DNA double-strand breaks. Nat. Commun. *13*, 5295. https://doi.org/10.1038/s41467-022-32743-w.

66. Kreitzer, F.R., Salomonis, N., Sheehan, A., Huang, M., Park, J.S., Spindler, M.J., Lizarraga, P., Weiss, W.A., So, P.L., and Conklin, B.R. (2013). A robust method to derive functional neural crest cells from human pluripotent stem cells. Am. J. Stem Cells *2*, 119–131.

67. Bajar, B.T., Lam, A.J., Badiee, R.K., Oh, Y.H., Chu, J., Zhou, X.X., Kim, N., Kim, B.B., Chung, M., Yablonovitch, A.L., et al. (2016). Fluorescent indicators for simultaneous reporting of all four cell cycle phases. Nat. Methods *13*, 993–996. https://doi.org/10.1038/nmeth.4045.

STAR★METHODS

KEY RESOURCES TABLE

REAGENT or RESOURCE	SOURCE	IDENTIFIER
Chemicals, peptides, and recombinant proteins		
ART558	Artios Pharma	N/A
NU7441	Selleckchem	Cat# S2638
XL413	Selleckchem	Cat# S7547
Alt-R S.p. Cas9 Nuclease V3	IDT	Cat# 1081058
Dimethyl Sulfoxide (DMSO)	VWR	Cat# 0231
Knockout DMEM	ThermoFisher Scientific	Cat# 10829018
Pen/Strep	ThermoFisher Scientific	Cat# 15140122
GlutaMAX	ThermoFisher Scientific	Cat# 35050061
Sodium Pyruvate	ThermoFisher Scientific	Cat# 11360070
MEM non-essential amino acids (NEAA)	ThermoFisher Scientific	Cat# 11140050
2-Mercaptoethanol	ThermoFisher Scientific	Cat# 31350010
Fetal bovine serum (mES cells)	Capricorn Scientific	Cat# FBS-12A
Fetal bovine serum (human cells)	Bodinco BV	Lot# BDC-16568
G418	Merck Millipore	345812
StemFlex medium	ThermoFisher Scientific	Cat# A3349401
Matrigel GFR Basement Membrane Matrix	Corning	Cat# 356231
RevitaCell Supplement	ThermoFisher Scientific	Cat# A2644501
StemPro Accutase Cell Dissociation Reagent	ThermoFisher Scientific	Cat# A1110501
Lipofectamine™ 2000	ThermoFisher Scientific	Cat# 11668019
Lipofectamine™ RNAiMAX transfection reagent	ThermoFisher Scientific	Cat# 13778100
Opti-MEM	ThermoFisher Scientific	Cat# 31985070
6-thioguanine	Sigma Aldrich	Cat# A4882
AMPure XP beads	Beckman Coulter	Cat# A63881
GoTaq DNA polymerase	Promega	Cat# M7841
Phusion High-Fidelity DNA Polymerase	ThermoFisher Scientific	Cat# F530L
Critical commercial assays		
PrimeSTAR GXL kit	Takara	Cat# R050B
Quant-iT dsDNA assay kit	ThermoFisher Scientific	Cat# Q33120
SMRTbell Express Template Prep Kit 2.0	PacBio	Cat# 100-938-900
High Sensitivity DNA chip	Agilent	Cat# 5067–4626
Sequel® II sequencing kit 2.0	PacBio	Cat# 101-820-200
DNeasy Blood and Tissue Kit	Qiagen	Cat# 69504
P3 Primary Cell 4D-Nucleofector X Kit	Lonza	Cat# V4XP-3024
Deposited data		
Raw targeted sequencing data (short- and long-read)	This manuscript	NCBI SRA database, accession code PRJNA799878
Experimental models: Cell lines		
Mouse: 129/Ola-derived IB10 mES cells	Schimmel et al.[36]	N/A
Mouse: IB10 wild-type HPRT-GFP knock-in mES cells (2 clones)	Schimmel et al.[36]	N/A
Mouse: IB10 Polq$^{-/-}$ HPRT-GFP knock-in mES cells (2 clones)	Schimmel et al.[36]	N/A

Continued

REAGENT or RESOURCE	SOURCE	IDENTIFIER
Mouse: IB10 Ku80⁻/⁻ HPRT-GFP knock-in mES cells (2 clones)	Schimmel et al.[36]	N/A
Mouse: IB10 wild-type GFP-Rosa targeted cells	This manuscript	N/A
Mouse: IB10 Polq⁻/⁻ GFP-Rosa targeted cells	This manuscript	N/A
Mouse: IB10 Ku80⁻/⁻ GFP-Rosa targeted cells	This manuscript	N/A
Human: HEK293T cells	Common lab stock	N/A
Human: U2OS cells	Common lab stock	N/A
Human: HeLa cells	Common lab stock	N/A
Human: RPE1-hTERT cells	Gift from Rob Wolthuis	N/A
Human: iPS cell-line WTC-11	Coriell Institute	Cat# GM25256
Oligonucleotides		
Human HPRT_ex3.2 L65F-G70E HDR template (5′- TGAACGTCTTGCTCGAGATGTGATGAAG GAGATGGGAGGCCATCACATTGTAGCTTTC TGTGTGCTCAAGGAGGGCTATAAATTCTTT GCTGACCTGCTGGATTACATCAAAGCACT GAA-3′)	IDT, Ultramer	N/A
BFP HDR template (mES cells) (5′- TCTGCACC ACCGGCAAGCTGCCCGTGCCCTGGCCCACC CTCGTGACCACCCTGACGCATGGCGTGCAG TGCTTCAGCCGCTACCCCGACCACATGAAG CAGCACGACTTCTTCAAGTCCG-3′)	IDT, Ultramer	N/A
BFP HDR template (human iPS cells) (5′- ACCCT GAAGTTCATCTGCACCACCGGCAAGCTGCCC GTGCCCTGGCCCACCCTCGTGACCACCCTG AGCCACGGGGTGCAGTGCTTCAGCCGCTAC CCCGACCACATGAAGCAGCACGACTTCTTCA AGTCCGCCATGCC-3′)	IDT, Alt-R HDR Donor Oligo	N/A
See Table S1 for additional cloning and sequencing oligonucleotides	This paper	N/A
Recombinant DNA		
pU6-(BbsI)_CBh-Cas9-T2A-mCherry	Laboratory of Ralf Kuehn	Addgene #64324
px459_spCas9-2A-iRFP670	Gift from Bert van de Kooij[65]	N/A
px459_spCas9-Geminin-2A-iRFP671	Gift from Bert van de Kooij	N/A
px459_spCas9-HE-2A-iRFP671	Gift from Bert van de Kooij	N/A
px459_spCas9-2A-i53-2A-iRFP671	Gift from Bert van de Kooij	N/A
eGFP-P2A-Neomycin-HPRT targeting vector	Schimmel et al.[36]	N/A
CAG-eGFP-Neomycin-Rosa targeting vector	Gift from Conny Brouwers and Sjef Verbeek	N/A
Software and algorithms		
TIDER	Brinkman et al.[42]	https://shinyapps.datacurators.nl/tider/
NovoExpress (version 1.4.1)	Agilent	N/A
BD FACSDiva software (version 9.0.1)	BD biosciences	N/A
Graphpad Prism (v9.3.1)	Graphpad	N/A
SIQ	van Schendel et al.[1]	https://github.com/RobinVanSchendel/SIQ
SIQPlotteR	van Schendel et al.[1]	https://siq.researchlumc.nl/SIQPlotter/
Other		
Alt-R CRISPR-Cas9 tracrRNA	IDT	Cat# 1072534

(Continued on next page)

Continued

REAGENT or RESOURCE	SOURCE	IDENTIFIER
Alt-R CRISPR-Cas9 crRNA HPRT ex3.2 (/AltR1/ rArGrCrCrCrCrCrUrUrGrArGrCrArCrArCrArGr GrUrUrUrUrArGrArGrCrUrArUrGrCrU/AltR2/)	IDT	N/A
Alt-R CRISPR-Cas9 crRNA eGFP (AltR1/rGrCrUr GrArArGrCrArCrUrGrCrArCrGrCrCrGr UrGrUrUrUrArGrArGrCrUrArUrGrCrU/AltR2)	IDT	N/A

RESOURCE AVAILABILITY

Lead contact
Further information and request for resources and reagents should be directed to and will be fulfilled by the lead contact, Marcel Tijsterman (m.tijsterman@lumc.nl).

Materials availability
Reagents generated in this study can be made available on request.

Data and code availability
- The raw targeted sequencing data generated in this study have been deposited in the NCBI SRA database under accession code PRJNA799878. A description of the sequence files can be found in Table S2.
- Sequencing data has been analyzed using SIQ software.[1] This paper does not report original code.
- Any additional information required to reanalyze the data reported in this paper is available from the lead contact upon request.

EXPERIMENTAL MODEL AND SUBJECT DETAILS

Cell culture and cell lines
The 129/Ola-derived IB10 mouse embryonic stem (mES) cell lines were maintained on 0.1% gelatin-coated dishes in Buffalo rat liver (BRL)-conditioned KnockOut DMEM (Gibco) supplemented with 100 U/mL penicillin, 100 μg/mL streptomycin, 2 mM GlutaMAX, 1 mM sodium pyruvate, 1× non-essential amino acids, 100 μM β-mercaptoethanol (all from Gibco), 10% fetal calf serum (Capricorn Scientific) and leukemia inhibitory factor. The HPRT-eGFP stable wild-type, $Polq^{-/-}$ and $Ku80^{-/-}$ mES cell-lines have been previously described.[36] To obtain monoallelic GFP-Rosa positive mES cell-lines, wild-type, $Polq^{-/-}$ and $Ku80^{-/-}$ cells were transfected with *Pvu*I linearized CAG-eGFP-Neomycin plasmid containing homology arms to target the Rosa locus (kind gift from Conny Brouwers and Sjef Verbeek). Cells were seeded in 10cm dishes and 24 hours post transfection medium was replaced for fresh medium containing 200 μg/mL G418 (Millipore). Clones were allowed to grow and picked after 7–10 days; monoallelic targeted clones were selected by PCR analysis (Figure S4A). Human RPE1-hTERT (gift from Rob Wolthuis), HEK293T, HeLa and U2OS cells were cultured in DMEM supplemented with GlutaMAX (Gibco), 10% fetal calf serum (Bodinco BV) and penicillin/streptomycin (Sigma). The human induced pluripotent stem (iPS) cell line WTC-11 (Coriell Institute, #GM25256[66]), in which an EGFP sequence was integrated at the AAVS1 locus, were maintained in StemFlex Medium (Gibco, A3349401) on plates coated with Matrigel GFR Basement Membrane Matrix (Corning, 356231). All cell-lines were grown at 37°C and 5% CO_2 and were frequently tested negative for mycoplasma contamination.

METHOD DETAILS

Chemicals
ART558 [33] (Artios Pharma) was dissolved as 10 mM stock in DMSO and used at 10 μM or as indicated. NU7441 (Selleckchem) was dissolved as 5 mM stock in DMSO and used at 2 μM. Equal amounts of DMSO were added in (mock-)treated cells in all experiments. XL413 (Selleckchem) was dissolved as 10 mM stock in SQ and used at 10 μM.

Plasmids
Plasmid pU6-(BbsI)_CBh-Cas9-T2A-mCherry was a gift from Ralf Kuehn (Addgene plasmid #64324). The pspCas9-2A-iRFP670, pspCas9-Geminin-2A-iRFP670, pspCas9-HE-2A-iRFP670 and pspCas9-2A-i53-iRFP670 constructs used in Figure S5 were a gift from Bert van de Kooij. The pspCas9-2A-iRFP670 construct was previously described.[65] The Geminin, HE and i53 sequences were derived from addgene plasmids #83841, #109400 and #74939[22,43,67] respectively, and cloned into pspCas9-2A-iRFP670 using Gibson assembly. To obtain Cas9-sgRNA expressing constructs, two complementary oligonucleotides (Integrated DNA Technologies) containing the target sequence and *Bbs*I overhangs were phosphorylated, annealed, and cloned into BbsI digested Cas9

backbone plasmids. An overview of the targeted sequences can be found in Table S1. The eGFP-P2A-Neomcyin plasmid containing homology arms to target the *HPRT* locus was previously described.[36]

Transfections

mES cells were trypsinized, counted, and resuspended in knockout DMEM (Gibco) and transfected in suspension using Lipofect-amine 2000 (Invitrogen):DNA ratio of 2.4:1. In general, 1.5×10^6 cells were transfected using 2 µg of total DNA and incubated for 30 min at 37°C and 5% CO2 in round-bottom tubes, subsequently cells were seeded on gelatin-coated plates containing BRL-conditioned medium and indicated inhibitors or DMSO. Human RPE1-hTERT, HEK293T, HeLa and U2OS cells were trypsinized, counted, and resuspended in Opti-MEM (Gibco); 0.6×10^6 cells were transfected in suspension using Lipofectamin 2000 (Invitrogen):DNA ratio of 2.4:1 (RPE1-hTERT, HeLa and U2OS) or 3.4:1 (HEK293T) and incubated for 30 min at 37°C and 5% CO2 in round-bottom tubes. Cells were subsequently seeded in Opti-MEM containing indicated inhibitors or DMSO. Medium was refreshed 24 hours post-transfection; inhibitors were left on the cells for five days. For experiments with ssDNA repair templates in mES, HEK293T, HeLa or U2OS cells (Figures 4A–4C and 4E respectively), 120 bp long Ultramer DNA oligos (IDT) were used containing ∼60 bp homology on both sites of the target-site and that contain the designed mutations (Table S1). Cells were transfected with a Cas9-sgRNA expressing plasmid and Ultramer in a 1:25 ratio (in general: 2.3 µg Cas9-sgRNA expressing plasmid and 1.85 µL of a 10 µM Ultramer stock). For the experiment with a ssDNA repair template in RPE1-hTERT cells (Figure 4E) and the HDR experiment in Figure S5D, 1.0×10^6 cells were transfected using 30 µL RNAiMAX (Invitrogen) in a transfection mixture containing 1250 µL OptiMEM (Invitrogen), 0.6 µL Cas9 enzyme (61 µM, IDT), 3,75 µL pre-assembled 10 µM sgRNA (duplexes formed with 100 µM Alt-R crRNA and 100 µM tracrRNA in nuclease-free duplex buffer, all from IDT and according to the manufacturer's protocol) and 3.75 µL of a 10 µM Ultramer stock).

HPRT-eGFP gene mutation assay

mES cells were transfected with a Cas9-WT-2A-mCherry construct, expressing indicated sgRNAs targeting the *HPRT-eGFP* gene and treated with 0, 1 or 10 µM ART558. Two days after transfection cells were passaged and a fraction was used to determine the transfection efficiency by measuring the percentage of mCherry-positive cells on a NovoCyte flow cytometer (ACEA Biosciences). Subsequently, the mutation frequency was analysed seven days post transfection by measuring the percentage of GFP-negative cells on the NovoCyte. The absolute mutation frequency was calculated by correcting for the transfection efficiency measured on day two.

Targeted sequencing of Cas9-induced repair outcomes

Cells were transfected with Cas9-WT-2A-mCherry constructs expressing indicated sgRNAs and harvested seven days post transfection for DNA isolation. Genomic DNA was isolated by lysing cell pellets into 10 mM Tris-HCL pH 7.5, 10 mM EDTA, 200 mM NaCl, 1% SDS and 0.4 mg/mL Proteinase K. Lysates were incubated at 55°C for 3–16 hours after which the lysis was neutralized by adding saturated NaCl and centrifugation at 4000 rpm for 30 minutes. DNA was precipitated and extracted by adding one volume of isopropanol to the supernatant followed by centrifugation, washing with 70% ethanol and resuspension in TE.

Samples for Illumina sequencing were prepared as previously described.[36] Briefly, primers specific for the targeted regions were selected (Table S1) that yield a ∼150–200 bp product on wild-type alleles and that contain adaptors for the p5 and p7 index primers (5′- GATGTGTATAAGAGACAG-3′ and 5′-CGTGTGCTCTTCCGATCT-3′ respectively). These primers were used to amplify the targeted region, PCR products were subsequently purified using magnetic AMPure XP beads (Beckman Coulter) according to the manufacturer protocol and DNA was eluted in 20 µL MQ. Flow-cell adaptor sequences were added by performing PCRs with 5 µL purified PCR-product and 0.3 µM of p5 and p7 index primers. The PCR products were purified with AMPure XP beads and eluted in 20 µL MQ. PCR samples were pooled at equimolar concentrations per target-specific PCR. The quality and quantity of these pools were analysed using a High Sensitivity DNA chip on a Bioanalyzer (Agilent) which was used to generate an equimolar library that was sequenced on a NovaSeq6000 (Illumina) by 150-bp paired-end sequencing.

For PacBio sequencing, *HPRT*-mutant cells were selected by seeding 500.000 cells in 6-thioguanine containing medium seven days post-transfection and allowed to grow for seven days. 5′ Amino Modifier C6 (5AmMC6) modified primers (IDT) were designed (Table S1) to yield a ∼3500 bp product on wild-type alleles and that are tailed with universal sequences (5′-5AmMC6/GCAGTCGAA CATGTAGCTGACTCAGGTCAC/Forward_sequence-3′ and 5′-5AmMC6/TGGATC-ACTTGTGCAAGCATCACATCGTAG/Reverse_ sequence-3′). These primers were used to amplify the targeted region in 25 µL reactions using the PrimeSTAR GXL kit (Takara) and the following conditions: 98°C for 30 s, 20 cycles of 95°C for 15 s, 60°C for 15 s and 68°C for 4 min, and the final extension 68°C for 7 min. Next, 2.5 – 3.5 ng round-one PCR product and Barcoded Universal Primers were used in a second-round PCR with PrimeSTAR GXL and the following conditions: 98°C for 30 s, 20 cycles of 95°C for 15 s, 64°C for 15 s and 68°C for 4 min, and the final extension 68°C for 7 min. DNA concentrations were measured using the Quant-iT dsDNA assay kit and the Qubit Fluo-rometer (both Thermo Fisher Scientific) according to the manufacturer's protocol and PCR samples were pooled at equimolar concentrations to contain 1000–2000ng of DNA in total, the quality of these pools were analyzed on the Femto pulse system (Agilent). SMRTbell library preparation was performed on 1000 ng purified PCR pool following the Procedure & Checklist - Amplicon Template Preparation and Sequencing (PN 100-815-000 Version 04, Pacific Biosciences) and using SMRTbell Express Template Prep Kit 2.0. The library was sequenced on Sequel II using sequencing primer V4, Sequencing kit 2.0 and Binding kit 2.0 on an 8M SMRT cell with a

movie time of 30 hr. Circular consensus sequences were generated with ccs version 6.0.0 (commit v6.0.0-2-gf165cc26) and barcodes were demultiplexed using lima 2.0.0 (commit v2.0.0).

Sequence analysis Cas9-induced repair outcomes

A custom JAVA program (https://github.com/RobinVanSchendel/SIQ) was used to filter and align NGS-sequence reads to a reference sequence containing the primer sequences and the CRISPR-Cas9 target sites.[1] High-quality reads (containing bases with error probability <0.08) were classified into the following groups: deletion, delins (deletion with an insertion of de novo DNA at the location of the deletion), insertion, 1 bp insertion, tins (templated insertion; events containing a ≥ 6 nt insertion with a large enough match to a DNA sequence in the immediate vicinity of the mutation junction (100 bp in both directions and orientation) with the probability of finding such a match of the same size in a scrambled sequence being <10%; for more detailed information see[1]), snv (single-nucleotide variant), wild-type (i.e. identical to the reference sequence). Wild-type and SNV reads were excluded from analysis: all data in the figures is analysed relative to the total amount of mutant reads. Additional parameters such as deletion/insertion-size and microhomology length for deletions were determined for each event. Finally, SIQPlotteR was used to generate plots of the mutational spectra.

HDR experiments mES cells

For the GFP to BFP conversion assay, GFP-Rosa mES cells were transfected with a Cas9-sgRNA expressing plasmid and a ssDNA repair template (Ultramer, IDT) in the presence of indicated inhibitors. Two days after transfection cells were passaged and a fraction was used to determine the transfection efficiency by measuring the percentage of mCherry-positive cells on a NovoCyte flow cytometer. Five days post transfection, the percentage of GFP$^+$, GFP$^-$ and BFP$^+$ cells was measured using a BD FACSAria III using BD FACSDiva software (BD Biosciences). The HDR/EJ ratio was calculated by dividing the amount of BFP$^+$ cells by the amount of GFP$^-$ cells. For the *HPRT-eGFP* knock-in assay, wild-type mES cells were transfected with a Cas9-sgRNA expressing plasmid and an eGFP-P2A-Neomcyin *HPRT*-targeting plasmid (circular or linearized by *Pvu*I) in a 1:1 ratio. Two days after transfection cells were passaged and a fraction was used to determine the transfection efficiency by measuring the percentage of mCherry-positive cells on a NovoCyte flow cytometer. Seven days post transfection, the knock-in frequency was determined by measuring the amount of GFP$^+$ cells on the NovoCyte. The absolute knock-in frequency was calculated by correcting for the transfection efficiency measured on day two.

HDR experiment human cells and TIDER analysis

HEK293T, HeLa or U2OS cells were transfected with a Cas9-sgRNA expressing plasmid and a ssDNA repair template (Ultramer, IDT) in the presence of indicated inhibitors or DMSO. RPE1ht cells were transfected with RNP-complexes and a ssDNA repair template in the presence of indicated inhibitors or DMSO. For the experiment in Figure S5D, HEK293T cells were transfected with RNP-complexes and a ssDNA repair template in the presence of indicated inhibitors or DMSO and co-treated for 24 hours with XL413. Two days after transfection cells were passaged and a fraction was used to determine the transfection efficiency by measuring the percentage of mCherry-positive cells on a NovoCyte flow cytometer. Six to eight days post transfection, cells were harvested and DNA was isolated. For TIDER analysis, primers specific for the targeted regions were selected (Table S1) to amplify a 368 bp long fragment using GoTaq (Promega). Targeted and untargeted control samples, together with a reference sequence containing the designed mutations (ordered as gBlock, IDT) were Sanger sequenced using the reverse primer. Sanger sequences were analyzed using the TIDER application[42] and these default settings: alignment window = 100 – 165, decomposition window = 155 – 255, indel size = 10. For the HDR experiment in human iPS cells, a 60–70% confluent well of a 6-well plate of undifferentiated hiPSC colonies was incubated with RevitaCell Supplement (Gibco) and indicated inhibitors or DMSO 1 hour prior to nucleofection. The ribonucleoprotein complex (RNP) was assembled by combining Alt-R S.p.Cas9-GFP V3 with sgRNA consisting of Alt-R crRNA and tracrRNA (all from IDT and according to the manufacturer's protocol). Sequences of sgRNA and ssODN2 template for GFP to BFP conversion were described previously (also see Table S1).[40] The RNP, 1 μM ssODN (IDT Alt-R HDR Donor Oligo) and 2 μM NU7441 and/or 10 μM ART588 were added to the nucleofection solution of the P3 Primary Cell 4D-Nucleofector X Kit (Lonza, V4XP-3024). hiPSCs were lifted from the plate using StemPro Accutase Cell Dissociation Reagent (Gibco) and nucleofected using program CA-137 of the Lonza 4D-Nucleofector X Unit. The nucleofected cells were transferred to one well of a 6-well plate per condition and expanded in presence of inhibitors or DMSO for one week. DNA was isolated using the DNeasy Blood and Tissue kit (Qiagen).

QUANTIFICATION AND STATISTICAL ANALYSIS

GraphPad Prism software (9.3.1) was used for statistical analysis. For mutation frequencies, a two-tailed unpaired t-test was used; replicate number, mean, error bars and p values are explained in the figure legends. For Figures 4B and 4D, Two-Way ANOVA with Dunnett's correction for multiple comparisons was used. Sample sizes (n) are indicated and represent biological replicates.